Expressivity Limits of Quantum Reservoir Computing

Nils-Erik Schütte,[1, 2] Niclas Götting,[1] Hauke Müntinga,[2] Meike List,[2, 3] Daniel Brunner,[4] and Christopher Gies[1]

[1]*Carl von Ossietzky Universität Oldenburg, Fakultät V, Institut für Physik, 26129 Oldenburg, Germany*
[2]*DLR, Institute for Satellite Geodesy and Inertial Sensing, Am Fallturm 9, 28359 Bremen, Germany*
[3]*University of Bremen, 28359 Bremen, Germany*
[4]*Institut FEMTO-ST, Université Franche-Comté CNRS UMR 6174, Besançon, France*

We investigate the fundamental expressivity limits of quantum reservoir computing (QRC) by establishing a formal connection to parametrized quantum circuit quantum machine learning (PQC-QML). We analytically prove, and numerically corroborate, that in QRC the number of orthogonal non-linear functions that can be generated from classical data is bounded linearly by the number of input encoding gates, independent of the reservoir's Hilbert space size. This finding applies across both physical and gate-based reservoir implementations using typical single-qubit input rotation schemes. Our results challenge the common assumption that exponential Hilbert space scaling confers a corresponding computational advantage in QRC, and demonstrate that true quantum benefit will require either more sophisticated, potentially multi-qubit, input schemes or quantum-native input data. These insights lay new groundwork for the design and evaluation of future QRC hardware and algorithms.

I. INTRODUCTION

The pursuit of quantum advantage in information processing has motivated the development of quantum machine learning (QML) algorithms and methods, which leverage quantum circuits or dynamical quantum systems to offer potentially exponential speedup or capacity over classical methods. Interest in QML has further increased as meaningful computation involving quantum circuits became possible on existing quantum hardware. In contrast to well recognized algorithms like Shor and Grover [1–3], the so-called ansatz in QML requires few gate operations only, minimizing gate-fidelity and qubit coherence-time requirements imposed by algorithmic quantum computing. The gate-based approach to QML leverages parameterized circuits that are adjusted to minimize a cost function, which can be viewed as iterative topology improvements of the quantum computing circuit [4–6]. We refer to this approach as parametrized quantum circuit quantum machine learning (PQC-QML). Seemingly unrelated, another QML approach called quantum reservoir computing (QRC) has emerged from the origin of artificial neural networks that harnesses the inherent dynamics of quantum systems for predicting non-linear functions of input data. In reservoir computing, the interconnects between the input and the neurons as well as among the neurons themselves are not trained but remain fixed, and learning is performed only at the generation of the output in a linear layer. Belonging to the class of recurrent neural networks, QRC is being considered especially for processing time-series data [7–10], albeit classification has also been demonstrated [11]. The key motivation is to harvest the exponential scaling in Hilbert-space dimensionality, as to compared a linear relationship between dimensionality and number of hardware neurons in classical physical hardware systems.

QRC has been around for a much shorter time than PQC-QML, and its predictive capabilities have not yet been explored in the same depth. Over the past years,

QRC performance has been gauged using measures based on dimensionality [12–15], short-term memory capacity [16–18] as well as a variety of non-linear benchmark tasks [7, 8]. Furthermore, benefits as well as the usual physical substrate-induced challenges faced when leveraging physical quantum effects for computing have been investigated in the QRC context, studying the impact of dissipation [7, 18–20], entanglement [14], quantum phases [21] and coherence [22]. These studies identified correlations between the reservoir's quantum properties and fundamental performance characteristics. However, a clear measure of the expressiveness as well as its analytically derived upper bound in QRC is still lacking.

In this work, we explore the number of leveraged quantum mechanical Hilbert-space dimensions of QRC in terms of its expressiveness, hence studying QRC's potential advantage due to quantum resources. This measure corresponds to the number of independent non-linear components that can be generated from the input data [23–27]. To access the expressiveness and the dimensionality in QRC, we establish a formal connection between the time evolution of the dynamical quantum system and the language of unitary gate operations in PQC-QML, for which Schuld *el al.* have determined the expressivity [28]. To analyze the dimensionality used in QRC, we use input encoding schemes that are currently being considered in the literature of QRC, i.e., during each data-point injection step, each qubit is either driven by the input using a single-qubit Pauli rotation around a randomly sampled axis [18, 29, 30], or via projective measurements [7, 31, 32]. Analytically, we derive an upper expressivity limit depending on the number of used Pauli rotations encoding the input. Counterintuitively, we find that this upper bound is predominantly independent of the reservoir itself. Using these particular input encoding schemes, the desired super-linear dimensionality scaling with the number of QRC qubits cannot materialize.

These findings fundamentally challenge the view that QRC can, by virtue of its exponentially large Hilbert space,

outperform classical reservoir computers in expressivity. Instead, our results point toward input encoding as the primary bottleneck, and motivate future QRC designs that exploit multi-qubit encoding or utilize native quantum inputs.

The paper is organized as follows. In Sec. II we establish a formal connection between QRC and PQC-QML in the language of quantum gates and transfer the methods of the latter to the time-dependent physics of reservoir computing. In Sec. III we quantify the expressive power of the QRC framework. In particular, we give an upper bound for the expressivity in dependence on the input encoding. Here, we also apply the expressivity analysis explicitly to a physical system used as reservoir, i.e., the transverse-field Ising model. Finally, in Sec. IV, the physical reservoir is compared to custom gate-based ansätze by calculating expressivities of both approaches, while also considering the influence of quantum mechanical measurement statistics.

II. FORMAL LINK OF QUANTUM RESERVOIRS TO GATE-BASED QUANTUM COMPUTERS

We begin by unraveling the close connection between the QRC scheme and the gate-based quantum computing architecture for multiple reasons. Firstly, it has the illustrative purpose of showing that a gate-based quantum computer allows us not only to vary the size of the reservoir via the number of qubits, but also the time evolution of the system by changing the unitary reservoir gate U_{res}. Secondly, by showing that the dynamics of every quantum reservoir can be mapped onto the language of quantum gate operations, we are able to apply expressivity measures known from PQC-QML to the concept of QRC. We explicitly exploit this connection in Sec. III to give an upper bound for the expressivity of the QRC framework. Thirdly, due to the possibility of quantum circuit design, the gate-based architecture can be considered an appropriate alternative for physical quantum systems.

In order to validate our approach we develop two different, complementary treatments of the same system. We first follow the common choice of representing the quantum reservoir by a transverse-field Ising model (TFIM) [7, 8, 14], as it contains the central aspects of a quantum artificial neural network while keeping the effort for simulation moderate. The system's Hamiltonian is given by ($\hbar = 1$) [7, 33, 34]:

$$H = h \sum_{i=1}^{N} \sigma_z^{(i)} + \sum_{i<j} J_{ij} \sigma_x^{(i)} \sigma_x^{(j)} \quad , \qquad (1)$$

where $2h$ is the energy difference between the ground and excited state and $\sigma_s^{(i)}, s \in \{x, y, z\}$ are the single-qubit Pauli matrices of the i-th qubit. The coupling matrix J_{ij} is initialized uniformly and randomly by sampling from the interval $[-1, 1]$ and then normalizing the values such that the spectral radius corresponds to the *coupling*
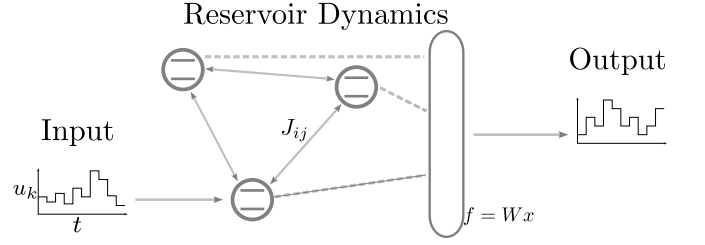

Figure 1: Schematic illustration of our used QRC setup: The three-qubit TFIM is driven by a random input sequence $u_k \in [0, 1]$ and evolves under the unitary time evolution determined by its underlying Hamiltonian, as given in Eq. (4). Information is extracted via $\sigma_z^{(i)}, i \in \{0, 1, 2\}$ measurements on all qubits.

strength J_0, which is a parameter. The state of the N qubit system is described by a density matrix $\rho \in \mathbb{C}^{2^N \times 2^N}$.

We consider a discrete time input signal $u_k \in [0, 1]$. The input values are encoded via state initialization, which is realized by the completely positive trace-preserving (CPTP) map

$$\rho \mapsto |\psi_{u_k}\rangle \langle \psi_{u_k}| \otimes \text{Tr}_1[\rho] \quad , \qquad (2)$$

with $|\psi_{u_k}\rangle = \sqrt{1 - u_k} |0\rangle + \sqrt{u_k} |1\rangle$ being the input-encoding state and Tr_1 denoting the partial trace over the input qubit, which is w.l.o.g. taken to be qubit 1. Hence, at this stage we connect only qubit 1 of the QRC to the external drive according to input information u_k. Later on, we will generalize away from this particular input injection and use an input connectivity onto multiple qubits with most general single-qubit rotations. Inputs are injected into the reservoir at time steps of duration Δ_t. The time evolution of the system is given by the unitary operator U_{Δ_t}

$$U_{\Delta_t} = \text{e}^{-iH\Delta_t} \quad , \qquad (3)$$

$$\rho \mapsto U_{\Delta_t} \rho U_{\Delta_t}^\dagger \quad . \qquad (4)$$

As readouts, we use σ_z measurements on all qubits and employ V-fold temporal multiplexing to get a readout dimension of NV [35]. Thus, the time step between two readouts is Δ_t/V. Such as it would be present in a physical implementation due to interactions with the environment, we consider a pure dephasing mechanism, and all qubits are subject to the single-qubit dephasing map [7]:

$$\rho \mapsto \frac{1 + \text{e}^{-2\gamma\Delta_t/V}}{2} \rho + \frac{1 - \text{e}^{-2\gamma\Delta_t/V}}{2} \sigma_z^{(i)} \rho \sigma_z^{(i)} \quad (5)$$

with the dephasing rate γ. To simulate a continuous interaction with the environment, this qubit dephasing is applied at every multiplexing step Δ_t/V. The here employed QRC topology is schematically depicted in Fig. 1.

This overall QRC procedure natively translates into the language of quantum circuits. The states of the qubits
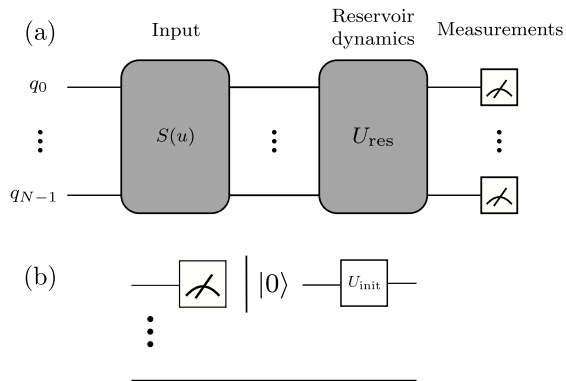
Figure 2: (a) Schematic figure illustrating the implementation of a QRC scheme on a gate-based quantum computer. The system is initialized in a random pure state. $S(u)$ is a unitary encoding the input into the quantum state, but this unitary can also be exchanged by the state initialization (non-unitary) as shown in (b). U_{res} represents the unitary time evolution of the used quantum reservoir, which is linear in any of the two cases.
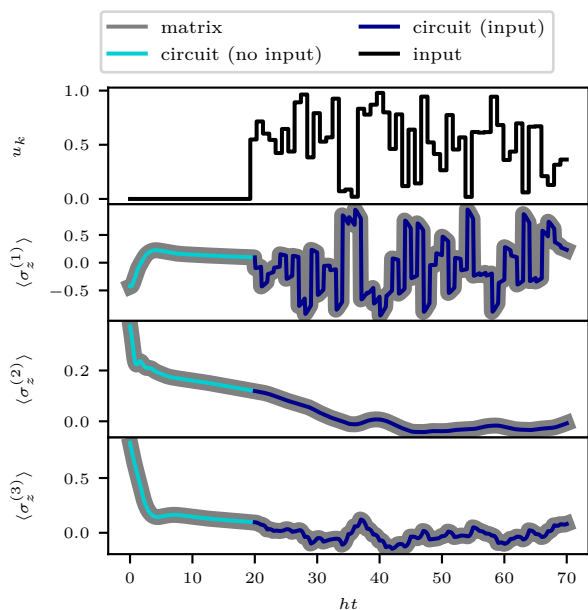

Figure 3: Input to the QRC and qubit dynamics ($\sigma_z^{(i)}$ expectation values) of the TFIM with qubit dephasing calculated with matrices and simulated with a gate-based quantum circuit model. Cyan data shows freely evolving qubit dynamics only with dephasing, while blue data shows dynamics under input injection.

in a quantum circuit are manipulated by unitary gate operations and measurements. Formally, an input encoding with qubit rotations and the time-evolution operator can therefore be written as unitary gate operations, as illustrated in Fig. 2. While $S(u)$ represents a unitary to encode the input, in this section, it has to be replaced with a non-unitary block implementing the state initialization as given in Eq. (2), which is shown in Fig. 2 (b). U_{res} displays the unitary reservoir dynamics given by the time-evolution operator in Eq. (3).

To compare this circuit model with results obtained from the reservoir dynamics according to Eq. (4), we consider the $\sigma_z^{(i)}$ qubit dynamics of a three qubit TFIM. The system is initialized in a random state and evolves freely until time $ht = 20$ only being subject to the dephasing. From $ht = 20$ onwards, a random scalar input sequence $\{u_k\}_k$ is injected into the reservoir according to Eq. (2), with Fig. 3 showing the resulting reservoir dynamics. Both approaches to the simulation of the TFIM yield identical qubit dynamics. This is only an example for the fact that any quantum system used as physical reservoir can equivalently be simulated on a programmable quantum computer. The main obstacle for practical implementation is the circuit depth of U_{res} on actual quantum computing hardware. Quantum computers possess a set of native gate operations that all other unitary gates are decomposed into. As an example, we have decomposed the TFIM unitary time evolution corresponding to one time multiplexing step Δ_t/V into the native gate set of the IBM kyiv device [36]. The resulting circuit is displayed in Fig. 8 of App. A. Clearly, a circuit for simulation of multiple time steps exceeds the feasible number of gate operations on current NISQ hardware, which lies in the range of a few hundred gates [37].

We note that the difficulties of simulating physical reservoirs on a gate-based architecture does not represent a drawback, since the primary motivation of RC is to harness the internal dynamics of physical systems rather than programming it. Still, establishing the link between both computing platforms enables us to use quantum circuits as reservoirs to analyze general aspects of QRC, which we will do in the following section to give an upper bound for the expressivity of the QRC framework.

III. LIMITS OF EXPRESSIVITY GIVEN BY THE INPUT ENCODING

To assess the expressive power of the QRC framework, we use a measure to quantify the expressivity in terms of the number of linearly independent functions a system can express. A QRC's expressivity depends on the way the input is injected into the dynamical system, as well as on the reservoir dynamics itself. We will investigate both dependencies and focus first on the former, while the latter will be covered in the next section.

The usual QRC procedure is displayed in Fig. 2. The system is initialized, the first input is injected and the reservoir dynamically evolves accordingly. This is followed either by the first measurement (since quantum mechanics does not allow a continuous monitoring of the states without back-action) or by the next cycle of input injection and reservoir dynamics. Hence, until the
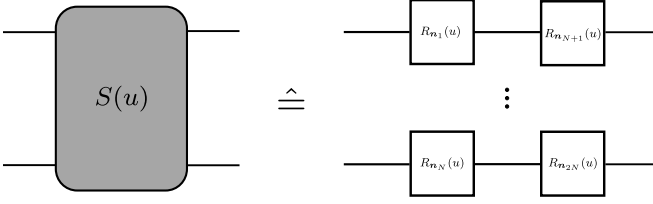
Figure 4: Illustration of the input injection with single-qubit rotations around arbitrary axes. The axes $R_{\boldsymbol{n}_i}$ through the Bloch sphere around each qubit state is rotated is randomly sampled independently for each qubit.

measurements are performed, the state of the system is changed in two ways, either by the input encoding or by the unitary reservoir dynamics. Although the input encoding has the ability to inject the input in a non-linear way (e.g. by single-qubit Pauli rotations) [38, 39], the unitary reservoir dynamics change the state's dependence on the input only in a linear fashion. While the input to the system changes in every cycle, the laws of transformation determining the reservoir dynamics stay the same. For example, considering input u_i of the i-th cycle, the reservoir cannot introduce a more complex dependency of the output features on the input u_i with just passing through more cycles. Because of this, it is sufficient to consider only one cycle of the QRC scheme in order to assess its expressivity.

Apart from this, we make three adaptions to our setup from Sec. II. Firstly, as we aim to determine an upper bound for the maximum number of linearly independent functions, we suppress the influence of dephasing. Secondly, information extraction from the reservoir is done by a positive operator-valued measure (POVM). We choose the n-th POVM element M_n to be a zero matrix with 1 at the n-th position on the diagonal, effectively measuring all diagonal elements of the density matrix. Since we are extracting exponentially many features, we make sure that the expressivity is not limited by the number of measured degrees of freedom. Thirdly, we address the input encoding. The injection procedure used in the previous section was firstly introduced in Ref. [7]. It was then adopted by many subsequent studies due to its simplicity by naturally incorporating noise into the system. However, this type of input injection drastically limits the output function space to a few non-linear functions [38]. Furthermore, an input encoding with a qubit-reset is not scalable to a majority of qubits of the system, because it collapses the the quantum state of these qubits, inhibiting any memory of the system. Therefore, the mostly used strategy for the input injection in the literature is a single-qubit rotation around one of the three Cartesian axes $\{x, y, z\}$, see e.g. Refs. [18, 29, 30]. We follow this common approach of single-qubit input gates as visualized in Fig. 4, with the generalization to rotations around arbitrary axes. The input gates are of the form $\mathrm{e}^{-\mathrm{i}uG}$, with an encoding Hamiltonian G being a summation of

Pauli matrices:

$$G = \frac{1}{2}(n_x\sigma_x + n_y\sigma_y + n_z\sigma_z) \quad , \qquad (6)$$

where the $n_i, i \in [x, y, z]$ are randomly sampled such that they fulfill $n_x^2 + n_y^2 + n_z^2 = 1$. The corresponding unitary gate can be decomposed into

$$
\begin{aligned}
R_n(u) &= \mathrm{e}^{-\mathrm{i}uG} \\
&= R_z(\alpha)R_y(\beta)R_z(u)R_y(-\beta)R_z(-\alpha) \quad ,
\end{aligned}
\qquad (7)
$$

with

$$
\begin{aligned}
\alpha &= \arctan2(n_y, n_x) \quad , \qquad (8)\\
\beta &= \arccos(n_z) \quad .
\end{aligned}
$$

A similar setup was used in Ref. [28], where the authors assumed a quantum model of the form

$$f_{\boldsymbol{\theta}}(u) = \langle 0 | U^{\dagger}(u, \boldsymbol{\theta})MU(u, \boldsymbol{\theta}) | 0 \rangle \quad , \qquad (9)$$

with $U(u, \boldsymbol{\theta})$ representing the quantum circuit which depends on the input u and some parameters $\boldsymbol{\theta}$, and M is an observable. In Ref. [28], Schuld and coworkers showed that this quantum model, given that the input is encoded by gates of the form $\mathrm{e}^{-\mathrm{i}uG}$, is given by a partial Fourier series

$$f_{\boldsymbol{\theta}}(u) = \sum_{\omega \in \Omega} c_{\omega}(\boldsymbol{\theta})\mathrm{e}^{\mathrm{i}\omega u} \quad , \qquad (10)$$

where the frequency spectrum Ω is solely determined by the eigenvalues of the encoding Hamiltonian G. Our QRC circuit resembles this setup except for the measurement. Instead of using a single observable, here, we use 2^N operators for the POVM measurement. Hence, we have a set of functions $\boldsymbol{f_{\theta}}(u) = \{f_{\boldsymbol{\theta}}^{(n)}(u)\}_n$, which all have the same structure of a partial Fourier series:

$$f_{\boldsymbol{\theta}}^{(n)}(u) = \sum_{\omega \in \Omega} c_{\omega}^{(n)}(\boldsymbol{\theta})\mathrm{e}^{\mathrm{i}\omega u} \quad . \qquad (11)$$

Using Pauli rotation gates for the encoding, Ref. [28] showed that the frequency spectrum Ω grows linearly with the number of input gates, i.e., r repetitions of single-qubit Pauli gates, either in parallel or sequentially, give rise to a truncated Fourier series of degree r. This means that the model represents a real Fourier series with r distinct frequencies. Therefore, each output from our QRC model, as given in Eq. (11) is such a truncated Fourier series of degree r. Since a real Fourier series of degree r can be decomposed into $2r+1$ orthogonal functions, consequently, the upper bound of the maximum possible number of linearly independent functions the QRC can express is given by

$$C_{\mathrm{T}}^{\max} = 2r + 1 \quad , \qquad (12)$$

where r is the number of Pauli rotations used for the input encoding. This simple formula carries an important

meaning, namely that the size of the output function space of any QRC approach is governed by the used input injection method and not by the reservoir itself. Hence, the expressivity in QRC cannot be improved by enlarging the Hilbert space of the underlying quantum-mechanical system. This is in stark contrast to RC with classical systems, where the available output function space can be drastically influenced by the complexity of the time dynamics or the size of the system.

We support this theoretical analysis with numerical simulations using the concept of the resolvable expressive capacity and eigentasks [25]. Within this framework, a quantum system is considered as an input-output map. Input $u \in \mathbb{R}$ is injected into the system and the output is obtained by a POVM, which measures K degrees of freedom X_k. The experimental issue of shot noise is accounted for by introducing the average values of stochastic features $X_k^{(s)}$ under S shots

$$\bar{X}_k(u) = \frac{1}{S} \sum_{s=1}^{S} X_k^{(s)}(u) \quad , \tag{13}$$

which allows one to calculate the resolvable expressive capacity (REC) C_T, according to Ref. [25]. The REC is a measure of the expressivity by quantifying how many linearly independent functions the system can express. These functions are called *eigentasks*, and C_T is the quantity for which we presented the upper bound in dependence of the input encoding in Eq. (12).

We support this finding by calculating the REC in dependence of the number of input encoding gates. We do this by neglecting measurement statistics (infinite shots) and extract the results of the POVM directly from the density matrix to facilitate a direct comparison with the theoretical upper bound. Furthermore, we compare the REC values of a product state possessing $U_\mathrm{res} = \mathbb{1}$ with a QRC model, where U_res is an entangling ansatz. The task of finding a good entangling ansatz is recognized as a central design element of PQCs in QML [40–42]. Since our main focus is not the design of a suitable gate-based reservoir, we choose already existing circuits that were introduced in Sim *et al.* [43] and reprinted in Appendix B for convenience.

For the following investigations, it is worthwhile to stress the difference between expressibility and expressivity. The former refers to the circuit's ability to explore the Hilbert space, i.e. how much of the Hilbert space can be covered by the circuit. The expressivity is a measure of how many linearly independent functions can be expressed at the output of a dynamical system.

For the purpose of investigating the dependence of the expressivity on the input encoding, we consider the entangling ansatz 6 from [43], see Appendix B, that produces a high expressivity.

The expressivity results of the product system and the one with this entangling ansatz are shown in Fig. 5. The quantum circuit with a single-qubit encoding via a rotation gate, as defined by Eq. (7), has access to a
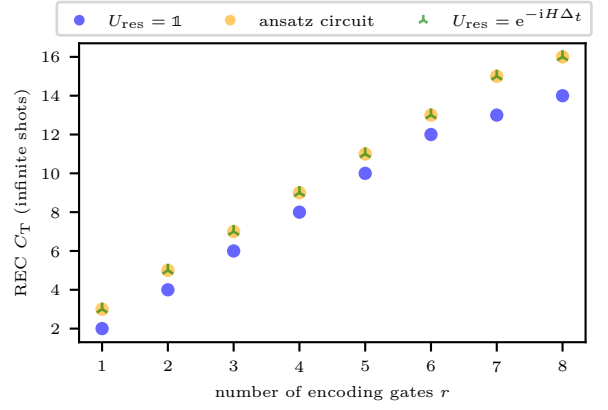

Figure 5: REC values for a QRC in dependence of the number of input encoding gates. The reservoir dynamics are realized by different unitaries: blue: identity, resulting in a product state system, orange: circuit 6 from Ref. [43], green: unitary time evolution of the TFIM. REC values are averaged values over 30 realizations of different sets of arbitrary input rotations. Results were obtained without shot noise (infinite shots).
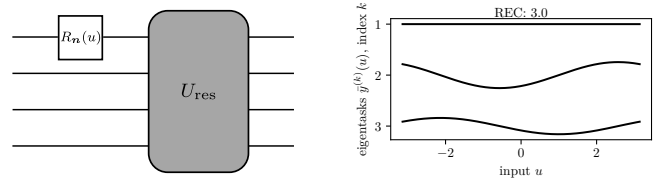

Figure 6: Left: Quantum circuit with a single input encoding gate using an entangling ansatz. Right: The corresponding eigentasks using circuit 6 in Fig. 9. The eigentasks are scaled for better visibility.

single frequency as presented in Ref. [28], which leads to a simple sine function as eigentask. Furthermore, the circuit can express a function that is independent of the input, i.e. a constant. This results in a REC of two, as fulfilled by the product state. The same circuit with one rotational input gate and an additional entangling layer has still access to a single frequency. The entangling layer enables the 'distribution' of the input information to other degrees of freedom. In this way, the circuit can construct an additional orthogonal function of the same frequency, which in this case is the cosine that appears in Fig. 6. For every rotational input gate that is added, the accessible frequency spectrum is extended by one frequency, increasing the number of eigentasks by two if an an entangling layer is being used. Hence, the input-gate-number dependent upper bound (Eq. (12)) is perfectly replicated by our REC calculations shown in Fig. 5.

An exception to this is the case of using eight encoding gates for the input injection, where Eq. (12) predicts a value of $C_\mathrm{T} = 17$. The reason for this is that the REC

value is not only limited by the number of input gates, but also by the number of the measured degrees of freedom as elaborated in Ref. [25]. The number of measured degrees of freedom is 16 in our setup due to the POVM on four qubits, restricting the REC to the same value.

Figure 5 also shows the expressivity in dependence of the number of input gates in product state systems. These systems feature a reduced expressivity, because the information is injected at the level of the individual qubits, in which case the output can only be composed as a superposition of an incomplete set of eigenvalues of the total many-particle system.

Reaching the upper bound in Eq. (12) is only possible if the entangling layer allows for the distribution of the input information into different degrees of freedom of the system. Consequently a layer of CNOT gates possesses the same REC value as the product state [25].

Up to now, the reservoir dynamics we investigated were realized by a gate-based ansatz circuit. Now, we apply the expressivity analysis also to the field of physical QRC. By using the methods from Sec. II, we therefore exchange U_{res} by the unitary time dynamics of a physical quantum system, chosen to be the TFIM. Hence, the setup is the same as depicted in Fig. 2 with $U_{\text{res}} = \text{e}^{-iH\Delta_t}$. The REC analysis reveals that the TFIM has the same dependence on the number of input gates as the gate-based ansatz circuit used before, which is also shown in Fig. 5. In a theoretical ideal scenario, the TFIM achieves the maximal possible expressivity. This agrees with our finding that the limits of expressivity in QRC depend on the input encoding procedure, rather than on the underlying system.

An important aspect that we have not yet considered is the presence of noise, which is always present in real-world implementations. Finite signal-to-noise ratios (SNRs) of the eigentasks prevent reaching this upper bound, leading to the question, which ansatz circuits maximize the expressivity under such conditions. In the following section, we investigate the expressivity of systems where we use the time evolution of the TFIM as reservoir in the presence of shot noise and compare it with different ansatz circuits.

IV. GATE-BASED ANSÄTZE FOR A QRC SCHEME

In this section we aim for a more realistic calculation of the expressivity and consider the impact of shot noise when performing a finite number of measurements to approximate expectation values. This will generally reduce the REC due to the finite signal-to-noise ratios (SNRs) of the eigentasks. The SNRs depend on the underlying system, in particular on the used reservoir.

Although, the idea of RC is to use physical systems as reservoir implementation rather than programmable
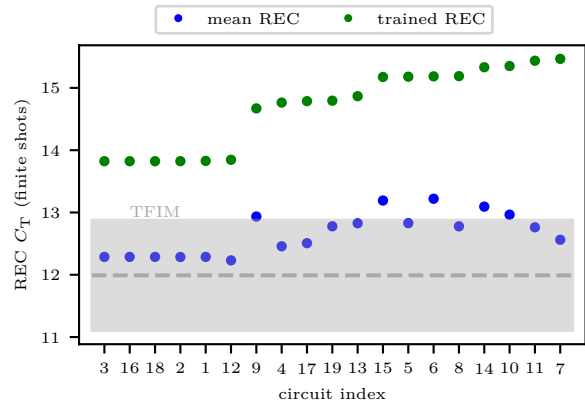

Figure 7: Expressivity values for different ansatz circuits and the TFIM. For all systems, input is injected via eight single-qubit rotations around randomly sampled axes. Blue: REC for different ansatz circuits. Values are calculated by randomly sampling circuits parameters (20 samples) and randomly sampling the parameters for the arbitrary rotations (30 samples) and averaging over the realizations. Green: REC values of the circuits with optimized, rather than randomly sampled, parameters. Parameters of the ansatz circuits have been optimized for a maximal expressivity. Dashed gray line indicates the expressivity of the non-optimized TFIM averaged over 20 reservoir realizations. Shaded gray area indicates the standard deviation.

(quantum) computers, the gate-based approach offers an opportunity to investigate the general properties of quantum systems in RC. Furthermore, the gate-based architecture could offer a more approachable platform for RC in the NISQ era. Here, we analyze the use of the different ansatz circuits from Sim *et al.* [43] (refer to Fig. 9) as reservoirs.

We calculated the REC values for all considered circuits using eight input encoding gates around randomly sampled axes. The results are shown in Fig. 7. As expected, a product state, as realized by circuit 1, has among the lowest expressivity. Circuit 2, which produces an entangled state via a single layer of CNOT gates, possesses the same expressivity. Again, this shows that entanglement alone is not the reason for a circuit to be expressive. Circuits 3, 16 and 18 also have a low expressivity, which could be explained by the fact that in these circuits the controlled rotations address the same degrees of freedom as the single-qubit rotations prior to them. Apart from that, the circuits 13 and 14 with controlled rotations perform quite well in general. For the expressivity, it seems to be beneficial if ansatz circuits have alternating parts between entangling gates and single-qubit rotations. Especially circuit 15, which uses solely CNOT gates for entanglement generation, shows a large improvement compared to circuit 3.

The shown results demonstrate that, in contrast to classical reservoirs and possibly against intuition, the

ability in QRCs to increase the output function space relies on the input encoding and not on the reservoir dynamics.

Once the reservoir introduces sufficient complexity for reaching the maximal expressivity allowed according to the input encoding, further increasing the size of the reservoir or its complexity cannot improve the expressivity. The expressivity is primarily determined by two factors: firstly by the way the input is injected as shown here, and secondly by the number of readouts that are performed [25]. The reservoir can only change the number of functions that are accessible, but the source for expressivity lies in the input injection. The set of non-linear orthogonal functions the reservoir has access to therefore is independent of the reservoir, since the time evolution in quantum mechanics is inherently linear.

Before concluding, we address the expressivity of the physical QRC that is also shown in Fig. 7 (dashed line shows average REC over 20 reservoir realizations). Interestingly, the TFIM has the lowest mean REC value among all tested reservoirs, performing even worse than the product-state circuit. We attribute this result to the specific dynamics produced by the time evolution of the TFIM, leading to output functions with smaller SNRs, thus lowering the expressivity. Besides the higher expressivity of the ansatz circuits, the gate-based approach to QRC has the additional advantage over physical reservoirs that their parameters can be precisely tuned and, therefore, be used for optimization. To do so, we employ an approach similar to parameterized quantum circuits in QML by performing an optimization step of the parameters of all ansatz circuits shown in Fig. 9 to maximize the attainable expressivity. The REC values for the optimized circuits are shown in green in Fig. 7. The results indicate that this approach generally improves the performance, although the increase in expressivity varies significantly among the individual quantum circuits. While the REC values of the worst performing circuits get a large increase after optimization, circuits 14 and 15 improve only slightly. Generally, after optimization there are less differences in the performance of the quantum circuits indicating that optimization is worthwhile in any case.

An open question remains how the SNRs of the eigentasks are affected by the specific choice of the circuit, which will be the topic of future investigations.

V. CONCLUSION

The central conclusion of our work is the counterintuitive fact that in physical reservoir computing, there is a fundamental difference between classical and quantum hardware platforms: While classical RC draws its capabilities from the complex non-linear dynamics that is inherent to the reservoir, quantum systems get their expressivity *not* from the reservoir. Instead, the power to express non-linear functions from the input data (expressivity) relies on the input encoding.

To reveal this fact, we have translated the QRC approach into the language of circuit-based QML, establishing a fundamental connection on an abstract level between these two very different QML paradigms. This analogy enables one to compare the expressivity of the TFIM as a representative for a physical QRC with a selection of different gate-based low-depth ansatz circuits. We find all of these ansatz circuits to outperform the TFIM if shot noise is taken into account, with the additional benefit that they can be optimized via their parametrization, which is generally not possible in a physical reservoir.

Our results challenge the widespread expectation of exponential computational advantage in QRC based solely on Hilbert space dimension, and instead highlight input encoding as the critical bottleneck to expressivity. We anticipate that overcoming this bottleneck will require new input injection paradigms or the use of quantum-native data, opening up new avenues for both experimental and theoretical exploration in the field.

Appendix A: Transpilation of the time evolution of the TFIM

Simulation of the TFIM on a gate-based quantum computer requires a transpilation of the unitary time evolution of the Ising system into the native gate set of the used quantum computer. As example, we transpiled the time-evolution operator, as given by Eq. (3), into the native gate-set of the IBM kyiv device. We performed the transpilation for a single multiplexing step of Δ_t/V. The transpiled circuit is shown in Fig. 8, illustrating the complexity of implementing the inherently simple time evolution of the TFIM on a gate-based device.

Appendix B: Ansatz circuits

For convenience, we show the ansatz circuits used by Sim *et al.* [43] and here in this work in Fig. 9.
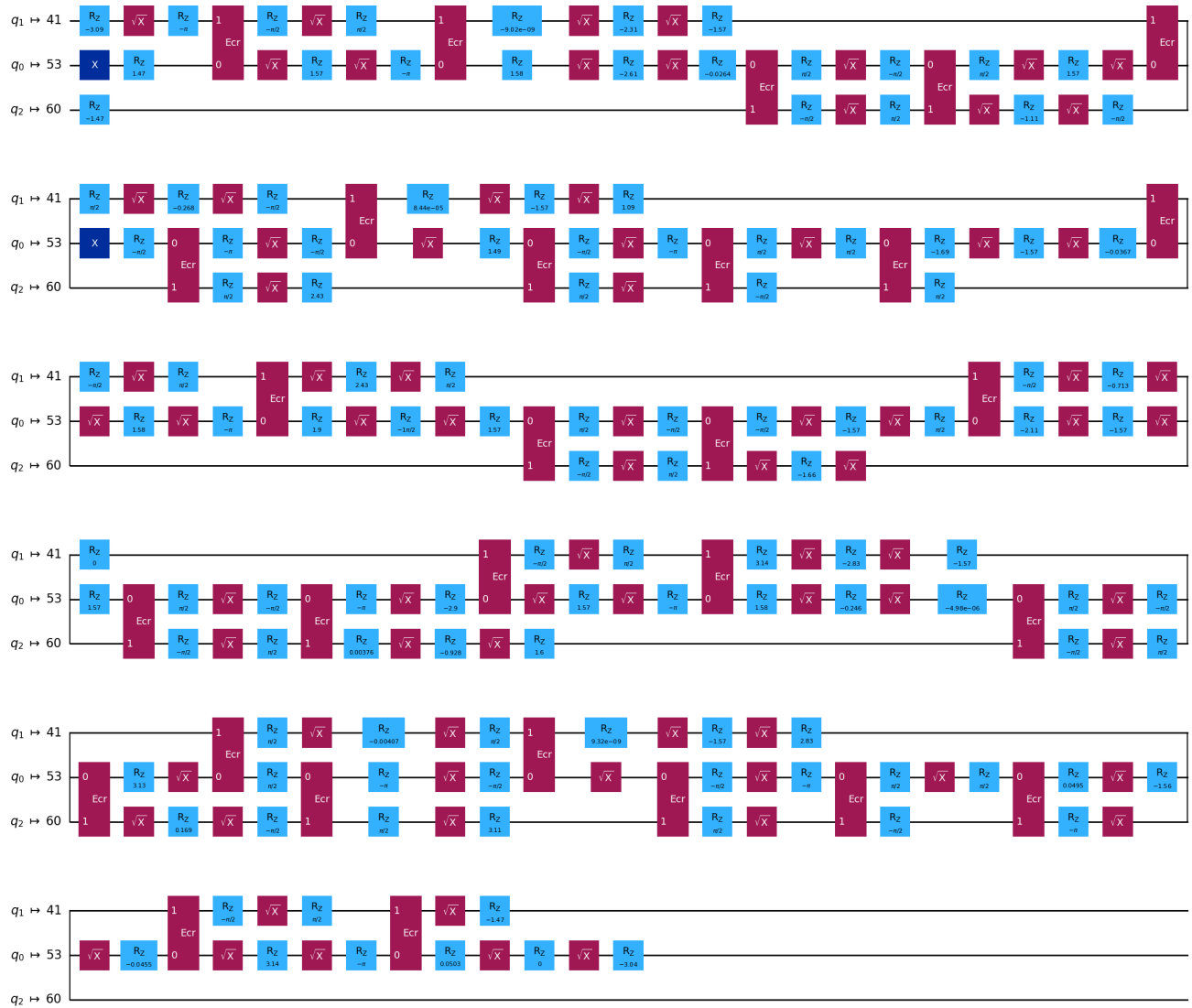
Figure 8: Transpiled circuit of the unitary which implements one time-multiplexing step of the TFIM. Transpilation was done with respect to the native gate set of the `ibm kyiv` device.
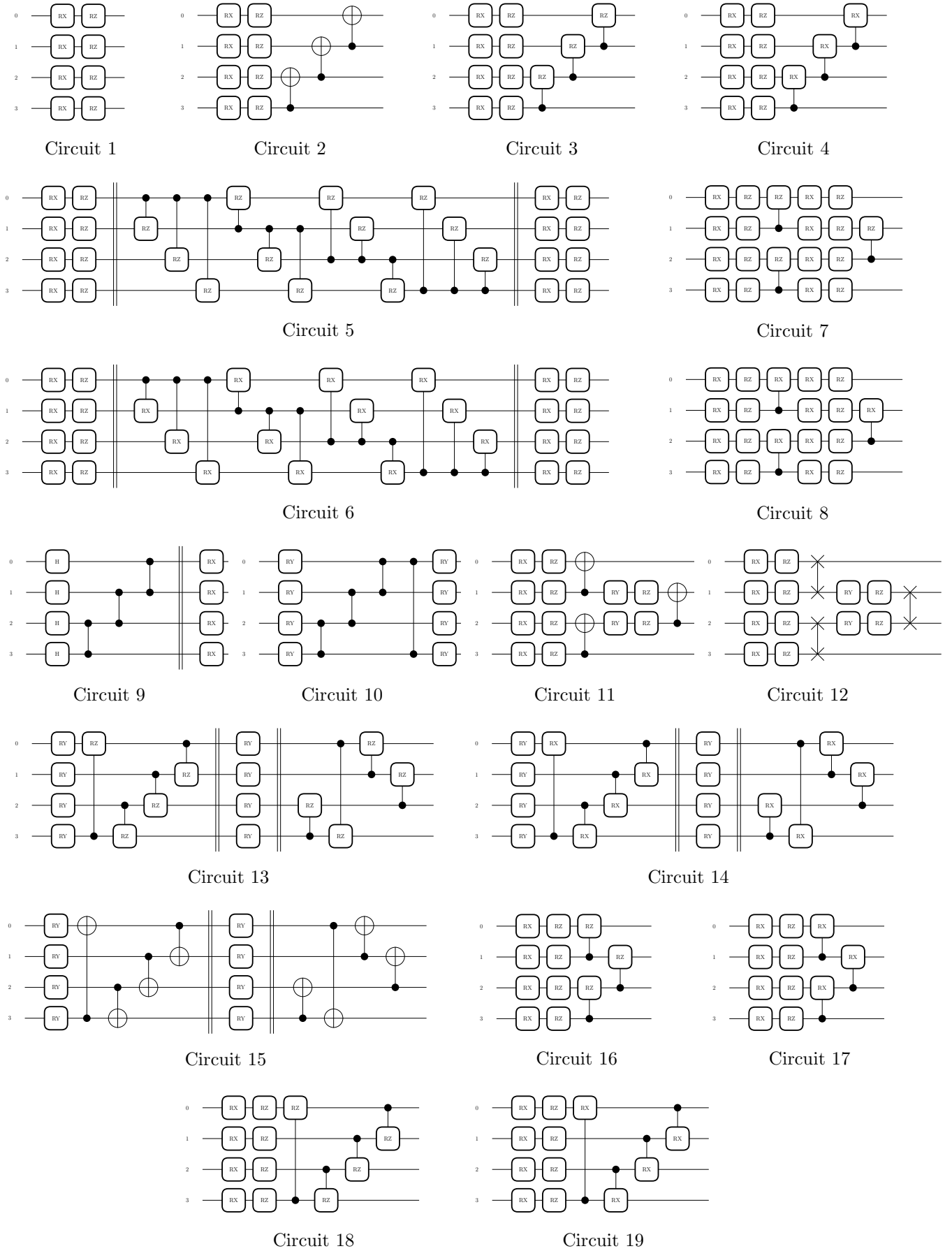
Figure 9: Ansatz circuits that are considered in the main text. The circuits are given in the same order as in [43] for better comparability.

[1] P. Shor, Algorithms for quantum computation: Discrete logarithms and factoring, in *Proceedings 35th Annual Symposium on Foundations of Computer Science* (IEEE Comput. Soc. Press, Santa Fe, NM, USA, 1994) pp. 124–134.

[2] P. W. Shor, Polynomial-Time Algorithms for Prime Factorization and Discrete Logarithms on a Quantum Computer, SIAM Journal on Computing **26**, 1484 (1997).

[3] L. K. Grover, A fast quantum mechanical algorithm for database search, in *Proceedings of the Twenty-Eighth Annual ACM Symposium on Theory of Computing - STOC '96* (ACM Press, Philadelphia, Pennsylvania, United States, 1996) pp. 212–219.

[4] K. Mitarai, M. Negoro, M. Kitagawa, and K. Fujii, Quantum circuit learning, Physical Review A **98**, 032309 (2018).

[5] M. Schuld and N. Killoran, Quantum Machine Learning in Feature Hilbert Spaces, Physical Review Letters **122**, 040504 (2019).

[6] V. Havlíček, A. D. Córcoles, K. Temme, A. W. Harrow, A. Kandala, J. M. Chow, and J. M. Gambetta, Supervised learning with quantum-enhanced feature spaces, Nature **567**, 209 (2019).

[7] K. Fujii and K. Nakajima, Harnessing Disordered-Ensemble Quantum Dynamics for Machine Learning, Physical Review Applied **8**, 024030 (2017).

[8] S. Čindrak, B. Donvil, K. Lüdge, and L. Jaurigue, Enhancing the performance of quantum reservoir computing and solving the time-complexity problem by artificial memory restriction, Physical Review Research **6**, 013051 (2024).

[9] J. Dudas, B. Carles, E. Plouet, F. A. Mizrahi, J. Grollier, and D. Marković, Quantum reservoir computing implementation on coherently coupled quantum oscillators, npj Quantum Information **9**, 64 (2023).

[10] P. Mujal, R. Martínez-Peña, G. L. Giorgi, M. C. Soriano, and R. Zambrini, Time-series quantum reservoir computing with weak and projective measurements, npj Quantum Information **9**, 16 (2023).

[11] Y. Suzuki, Q. Gao, K. C. Pradel, K. Yasuoka, and N. Yamamoto, Natural quantum reservoir computing for temporal information processing, Scientific Reports **12**, 1353 (2022).

[12] L. C. G. Govia, G. J. Ribeill, G. E. Rowlands, H. K. Krovi, and T. A. Ohki, Quantum reservoir computing with a single nonlinear oscillator, Physical Review Research **3**, 013077 (2021).

[13] G. Llodrà, C. Charalambous, G. L. Giorgi, and R. Zambrini, Benchmarking the Role of Particle Statistics in Quantum Reservoir Computing, Advanced Quantum Technologies **6**, 2200100 (2023).

[14] N. Götting, F. Lohof, and C. Gies, Exploring quantumness in quantum reservoir computing, Physical Review A **108**, 052427 (2023).

[15] S. Čindrak, L. Jaurigue, and K. Lüdge, Krylov Expressivity in Quantum Reservoir Computing and Quantum Extreme Learning (2024), arXiv:2409.12079 [quant-ph].

[16] H. Jaeger, Short Term Memory in Echo State Networks, Technical report (GMD-Forschungszentrum Informationstechnik (2001).

[17] K. Kobayashi, K. Fujii, and N. Yamamoto, Feedback-Driven Quantum Reservoir Computing for Time-Series Analysis, PRX Quantum **5**, 040325 (2024).

[18] A. Sannia, R. Martínez-Peña, M. C. Soriano, G. L. Giorgi, and R. Zambrini, Dissipation as a resource for Quantum Reservoir Computing, Quantum **8**, 1291 (2024), arXiv:2212.12078 [quant-ph].

[19] M. L. Olivera-Atencio, L. Lamata, and J. Casado-Pascual, Benefits of Open Quantum Systems for Quantum Machine Learning, Advanced Quantum Technologies , 2300247 (2023).

[20] Y. Kora, H. Zadeh-Haghighi, T. C. Stewart, K. Heshami, and C. Simon, Frequency- and dissipation-dependent entanglement advantage in spin-network Quantum Reservoir Computing (2024), arXiv:2403.08998 [quant-ph].

[21] R. Martínez-Peña, G. L. Giorgi, J. Nokkala, M. C. Soriano, and R. Zambrini, Dynamical Phase Transitions in Quantum Reservoir Computing, Physical Review Letters **127**, 100502 (2021).

[22] A. Palacios, R. Martínez-Peña, M. C. Soriano, G. L. Giorgi, and R. Zambrini, Role of coherence in many-body Quantum Reservoir Computing, Communications Physics **7**, 369 (2024).

[23] J. Dambre, D. Verstraeten, B. Schrauwen, and S. Massar, Information Processing Capacity of Dynamical Systems, Scientific Reports **2**, 514 (2012).

[24] A. Skalli, X. Porte, N. Haghighi, S. Reitzenstein, J. A. Lott, and D. Brunner, Computational metrics and parameters of an injection-locked large area semiconductor laser for neural network computing [Invited], Optical Materials Express **12**, 2793 (2022).

[25] F. Hu, G. Angelatos, S. A. Khan, M. Vives, E. Türeci, L. Bello, G. E. Rowlands, G. J. Ribeill, and H. E. Türeci, Tackling Sampling Noise in Physical Systems for Machine Learning Applications: Fundamental Limits and Eigentasks, Physical Review X **13**, 041020 (2023).

[26] M. Hary, D. Brunner, L. Leybov, P. Ryczkowski, J. M. Dudley, and G. Genty, Principles and Metrics of Extreme Learning Machines Using a Highly Nonlinear Fiber (2025), arXiv:2501.05233 [physics].

[27] A. M. Polloreno, Limits to Analog Reservoir Learning (2025), arXiv:2307.14474 [cs].

[28] M. Schuld, R. Sweke, and J. J. Meyer, Effect of data encoding on the expressive power of variational quantum-machine-learning models, Physical Review A **103**, 032430 (2021).

[29] S. Mifune, T. Kanao, and T. Tanamoto, Effects of dissipation in reservoir computing using spin qubit array, Japanese Journal of Applied Physics **64**, 04SP08 (2025).

[30] S. Tovey, T. Fellner, C. Holm, and M. Spannowsky, Generating Quantum Reservoir State Representations with Random Matrices (2025), arXiv:2404.07278 [quant-ph].

[31] A. Kutvonen, K. Fujii, and T. Sagawa, Optimizing a quantum reservoir computer for time series prediction, Scientific Reports **10**, 14687 (2020).

[32] R. Martínez-Peña, J. Nokkala, G. L. Giorgi, R. Zambrini, and M. C. Soriano, Information Processing Capacity of Spin-Based Quantum Reservoir Computing Systems, Cognitive Computation **15**, 1440 (2023).

[33] R. B. Stinchcombe, Ising model in a transverse field. I. Basic theory, Journal of Physics C: Solid State Physics **6**, 2459 (1973).

[34] P. Pfeuty and R. J. Elliott, The Ising model with a transverse field. II. Ground state properties, Journal of Physics C: Solid State Physics **4**, 2370 (1971).

[35] S. Sunada and A. Uchida, Photonic reservoir computing based on nonlinear wave dynamics at microscale, Scientific Reports **9**, 19078 (2019).

[36] IBM kyiv, https://quantum.ibm.com/services/resources?resourceType=current-instance&system=ibm_kyiv (2025).

[37] J. W. Z. Lau, K. H. Lim, H. Shrotriya, and L. C. Kwek, NISQ computing: Where are we and where do we go?, AAPPS Bulletin **32**, 27 (2022).

[38] P. Mujal, J. Nokkala, R. Martínez-Peña, G. L. Giorgi, M. C. Soriano, and R. Zambrini, Analytical evidence of nonlinearity in qubits and continuous-variable quantum reservoir computing, Journal of Physics: Complexity **2**, 045008 (2021).

[39] L. C. G. Govia, G. J. Ribeill, G. E. Rowlands, and T. A. Ohki, Nonlinear input transformations are ubiquitous in quantum reservoir computing, Neuromorphic Computing and Engineering **2**, 014008 (2022).

[40] M. Benedetti, E. Lloyd, S. Sack, and M. Fiorentini, Parameterized quantum circuits as machine learning models, Quantum Science and Technology **4**, 043001 (2019), arXiv:1906.07682 [quant-ph].

[41] Y. Du, T. Huang, S. You, M.-H. Hsieh, and D. Tao, Quantum circuit architecture search for variational quantum algorithms, npj Quantum Information **8**, 62 (2022).

[42] M. Pirhooshyaran and T. Terlaky, Quantum circuit design search, Quantum Machine Intelligence **3**, 25 (2021).

[43] S. Sim, P. D. Johnson, and A. Aspuru-Guzik, Expressibility and Entangling Capability of Parameterized Quantum Circuits for Hybrid Quantum-Classical Algorithms, Advanced Quantum Technologies **2**, 1900070 (2019).